

RESEARCH ARTICLE | AUGUST 15 2023

A search for chiral asymmetry in secondary electron emission from cysteine induced by longitudinally polarized electrons

Special Collection: [Chiral Induced Spin Selectivity](#)

K. J. Ahrendsen   ; K. W. Trantham  ; D. Tupa  ; T. J. Gay 



J. Chem. Phys. 159, 074301 (2023)

<https://doi.org/10.1063/5.0156419>



CrossMark

AIP Advances

Why Publish With Us?

 25 DAYS average time to 1st decision	 740+ DOWNLOADS average per article	 INCLUSIVE scope
---	--	---

[Learn More](#)



A search for chiral asymmetry in secondary electron emission from cysteine induced by longitudinally polarized electrons

Cite as: J. Chem. Phys. 159, 074301 (2023); doi: 10.1063/5.0156419

Submitted: 29 April 2023 • Accepted: 27 July 2023 •

Published Online: 15 August 2023



View Online



Export Citation



CrossMark

K. J. Ahrendsen,^{1,a)} K. W. Trantham,² D. Tupa,³ and T. J. Gay¹

AFFILIATIONS

¹Jorgensen Laboratory, University of Nebraska, Lincoln, Nebraska 68588-0299, USA

²University of Nebraska, Kearney, Nebraska 68849, USA

³Physics Division, Los Alamos National Laboratory, Los Alamos, New Mexico 87545, USA

Note: This paper is part of the JCP Special Topic on Chiral Induced Spin Selectivity.

a) Author to whom correspondence should be addressed: kahrendsen@smith.edu.

Now at: Department of Physics, Smith College, Northampton, Massachusetts 01063, USA.

ABSTRACT

We performed experiments searching for chirality-dependent secondary electron emission for a 141 eV longitudinally spin-polarized electron beam incident on a thick solid cysteine target. We determined the secondary electron yield by measuring the positive current produced when the cysteine target was negatively biased. No spin-dependent effects to a level of 10^{-3} were found for the secondary electron emission yield.

Published under an exclusive license by AIP Publishing. <https://doi.org/10.1063/5.0156419>

I. INTRODUCTION

The origins of biological homochirality have been the subject of much speculation for more than a century.¹ One hypothesis was put forward by Vester and Ulbricht in 1957 following the fall of parity.^{2,3} As originally stated, it argues that circularly polarized *bremstrahlung* resulting from the slowing in a matter of longitudinally spin-polarized cosmic ray electrons preferentially destroyed one handedness of biological precursors in the earth's primordial environment. A variant of this idea⁴ is that the polarized electrons themselves were the active agent in this chirally sensitive destruction, possibly through the channel of dissociative electron detachment (DEA).⁵

The feasibility of the latter mechanism was subsequently demonstrated by experiments that studied the preferential dissociation by DEA of chiral halocamphor targets with low-energy beams of longitudinally polarized electrons.⁶ Similar experiments have observed chiral sensitivity in the quasi-elastic scattering channel as well.⁷ It is fair to say that in all these measurements, no clear understanding of the actual electrodynamics of chiral interactions between polarized electrons and chiral molecules has emerged. There is a general consensus that interactions involving spin-orbit interactions

are important,⁸ but no comprehensive theory to support this idea yet exists. Given this situation, our experimental work has been guided by the idea that more data are needed for a broad range of collisional channels with different targets to search for unifying trends in chiral scattering. Any new experimental result, even a null one,^{9,10} provides some guidance in this endeavor.

A stronger connection between such experiments and the Vester-Ulbricht hypothesis would be made with the use of more biologically relevant targets. To this end, Göhler *et al.*¹¹ investigated the production of longitudinally spin-polarized electrons when unpolarized electrons were photoemitted from a gold substrate and traversed an oriented monolayer of DNA. Schaible *et al.*¹² have studied the interaction of polarized photoelectrons from a magnetized substrate with monolayers of L-histidine. Using XPS, they observed statistically significant chiral effects in the damaged cross-sections of these molecules. A potentially more promising candidate is cysteine, since it has a higher Z atom in it (S) that, through a spin-orbit coupling mechanism, could enhance chiral symmetries. Mondal *et al.*¹³ have shown that cysteine, bonded to a magnetized electrode, will act as a spin filter that can control electrochemical charge transfer rates. In an experiment similar to that described in the study by Schaible *et al.*, Rosenberg *et al.*¹⁰ used XPS to study chiral

differences in the polarized electron-induced chemistry of the cysteine layers chemisorbed on gold. No statistically conclusive effects were found.

In the experiments with halocamphor molecules in the gas phase,^{6,8} we used polarized electrons produced by photoemission from GaAs.¹⁴ In those experiments, the GaAs photocathodes proved susceptible to very low levels of contamination by the target molecules, although a beam bend and differential pumping were employed to isolate the chiral target from the photocathode. This contamination significantly reduced the lifetime of the photocathode's quantum efficiency, usually causing the electron source to fall below a useful photocurrent in 3–4 h. For this reason, in the experiments reported here, we have used a new type of polarized electron source based on Rb spin exchange^{15,16} that is immune to chemical contamination.

The electron beams produced by the Rb spin exchange source have a relatively broad energy width of 1–4 eV. We thus chose to study chiral interactions in a process that has not been investigated to date and that does not require a source of highly monochromatic electrons: kinetic secondary electron emission from solid targets. In such experiments with incident electron energies >100 eV, an energy spread of even 4 eV yields a negligible variation in the secondary electron yield. The photoemission of secondary electrons from gold and magnetized substrates has been used as a source to study electron chiral interactions with monolayers of ordered, handed molecules,^{10–12,17} and relatively large chiral effects (>1%) in the production of spin polarization or chemical reaction rates have been observed. (Chiral molecule gas-phase experiments with incident beams of polarized electrons generally find scattering asymmetries <0.1%.) No experiments, to date, however, have searched for chiral asymmetries in the production of secondary electrons from solids induced by incident electron beams. We report here the results of the first such experiment which uses solid, randomly oriented targets of cysteine.

Secondary electron production in the interaction of polarized electrons with solid chiral targets are arguably, more germane to the Vester–Ulbricht scenario of polarized cosmic ray electrons being slowed significantly in environments containing the precursors of biological molecules. This channel could exhibit a chirality dependence for a number of reasons. In standard theories of kinetic secondary electron emission,¹⁸ the incident electron travels into the solid, undergoing a series of quasi-elastic, excitation, and ionizing collisions. The combined cross-sections for these processes determine the stopping range for the incident electron and the average number of continuum electrons produced that can ultimately diffuse to the surface and be emitted as secondary electrons—typically one or two. All of these processes, in principle, can depend on the relative chirality of the incident electron and the target molecules, thus producing both a polarization-dependent range and a number of free electrons produced along the incident electron's track. The chiral sensitivity of the range has a second-order effect; the depth of an ionizing collision affects the probability of the ionized electron successfully diffusing to the surface. Although the nascent secondary electrons are not expected to be highly polarized, any residual polarization they might have could be expected to contribute to a chiral sensitivity in the total secondary electron yield.

It is not clear whether multiple scattering associated with secondary electron production could be expected to enhance or mask

chiral effects in the number of emitted electrons. Göhler *et al.*¹¹ have shown that transmission of electrons through large, oriented molecules such as DNA can produce surprisingly large effects, although the heaviest target atom is P ($Z = 15$), which should significantly diminish spin-orbit coupling. [The lowest Z in gas phase experiments to produce a measurable effect is Br ($Z = 35$).] On the other hand, the DNA molecules are oriented, and the transmission of electrons through the DNA films certainly involves multiple atomic collisions. Some combinations of these two factors presumably enhance any small spin-orbit chiral effects.

More generally, experiments conducted with randomly oriented molecular targets have the advantage that they yield a clean signature of chiral electron-molecule interactions. Experiments conducted with crystalline or oriented molecular targets may exhibit chiral effects that are artifacts of macroscopic chiral target geometry and that mask the more fundamental chiral interaction taking place.

For kinetic secondary electron emission to occur, the incident electrons must have sufficient energy to ionize multiple target atoms. This means that exchange interactions for the first few molecular collisions will not be important. Moreover, the relatively low Z atoms in cysteine cannot be expected to significantly depolarize the incident electron in its first several collisions. Thus, the primary electron's polarization might reasonably be expected to persist well into its total track length in the target.

II. APPARATUS

A. Spin-polarized electron source

The electron source is shown in Fig. 1 and described in more detail elsewhere.^{16,19} A beam of thermionic unpolarized electrons is directed onto a volume of optically pumped spin-polarized rubidium atoms. Through spin-exchange interactions or direct ionization, the transmitted electrons become spin-polarized. For this experiment, the 17(4)% longitudinally polarized beam had an energy of 141 eV with a FWHM of 4 eV. The electron polarization was flipped by changing the circular polarization of the pump laser used to polarize the rubidium. The pressure in the source chamber was 10^{-4} Torr when data were collected due to the 400 mTorr of N_2 buffer gas co-mingled with the Rb ($n_{Rb} \approx 10^{13} \text{ cm}^{-3}$) to facilitate the optical pumping process. This source chamber pressure resulted in energy-loss collisions that increased the energy distribution of the beam. A narrower energy width of 4 eV FWHM was obtained by applying a rejecting potential to an einzel lens in the differential pumping region. After passing through the differential pumping chamber, the beam was redirected to strike ~ 150 nm-thick targets of enantiomerically pure solid, randomly oriented cysteine. The target chamber vacuum was nominally 1×10^{-7} Torr, unless the helium target gas was introduced in the noble gas polarimeter for electron polarization measurements. In this case, the pressure increased to 1×10^{-4} Torr.

B. Target preparation

The cysteine targets were deposited on 0.5 in. diameter copper pin stubs that were coated with 150-nm thick layers of gold, applied by discharge sputtering. The gold coating readily binds with the thiol group in the cysteine.²¹ Copper also binds tightly with cysteine, but

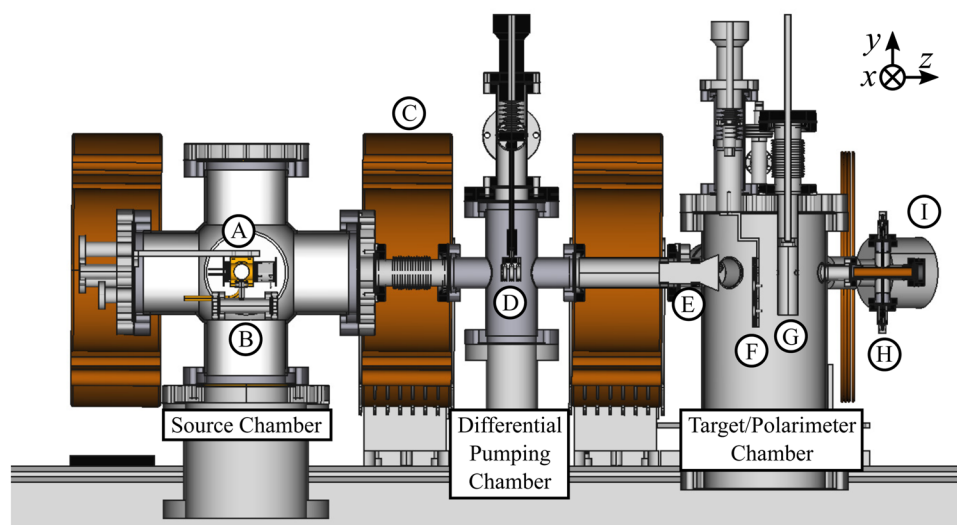


FIG. 1. The rubidium spin-exchange source.^{16,19} The spin-polarized electrons are generated in the source chamber at the left. In the collision cell (A), thermionically emitted unpolarized electrons interact with optically pumped Rb introduced from the reservoir (B). Spin-exchange processes yield a longitudinally polarized beam. The electrons then are guided to the target chamber on the right by a series of external solenoidal magnets (C). The target chamber contains a target holder (F) and a noble gas polarimeter²⁰ comprising a He target cell (G) and an optical polarimeter (I). A Faraday cup (H) acts as a beamstop. Deflector plates (E) switch the polarized electron beam between the chiral target and the He polarimeter and Faraday cup. The differential pumping region in the center separates the polarimeter and source buffer gases from each other and contains an einzel lens (D) to aid in beam transport and monochromatization.

studies have shown that copper atoms can migrate into the cysteine layer.²² We coated the pins with gold to avoid this.

For this study, we produced layers of cysteine thick enough that the incoming electrons would not reach the substrate (electron mean-free stopping distances in organic materials are at most 20 nm for incident energies between 100 and 200 eV²³), but thin enough that the incident charge would not substantially accumulate in the cysteine (see below). Pouring an aqueous solution directly on the pin to evaporate resulted in an inhomogeneous distribution of cysteine, with noticeable patches of thicker coverage. For this reason, we “painted” the solution onto the pins. This process involved heating the pin to a temperature of 130 °C, below the decomposition point of cysteine (160 °C²⁴). A 1M solution of cysteine was applied by ten strokes of a fine-bristled paintbrush to the surface of the pin. Surface profile measurements using a stylus surface profiling system indicated that this layer had a minimum thickness of ~150 nm, with “hills” as high as 600 nm. The samples were stored in a desiccator until they were loaded into the vacuum chamber. For a typical data collection run, we loaded two pins, one with each enantiomer of cysteine, into a carriage in the vacuum system. The carriage used a linear translation device to allow switching between pins without breaking the vacuum. As the device is illustrated in Fig. 1, the top pin is just below the apparatus’ central axis, and the electron beam is deflected down to hit it. The carriage system translates the bottom pin to the same spot to collect data on the opposite enantiomer.

C. Experiment description

The data collection procedure is summarized as follows. The electron polarization P_e and the Rb polarization and density, P_{Rb}

and n_{Rb} , respectively, were measured. The electron beam was then deflected onto the cysteine target. Vertical displacement of the beam was achieved using the principle of the trochoidal monochromator,²⁵ where the magnetic field in the direction of the beam pairs with a transverse electric field in the horizontal plane to cause deflection. The secondary electron emission asymmetry was measured by recording the current on the target for each polarization of the beam. This process was repeated for both the asymmetry signal measurement and the measurement of the instrumental asymmetry background. Following the measurement of these asymmetries, P_e was again measured to verify that it had not changed significantly.

The electron polarization was measured with a typical beam current of 200 nA using He optical polarimetry.^{20,26,27} Rb polarizations and densities were monitored by determining the Faraday rotation of a probe laser.^{19,28,29}

In the asymmetry runs, the current was reduced to ~15 nA to minimize the effects of charging the insulating cysteine target. Higher incident currents resulted in time-dependent currents measured on the targets themselves that often took hours to settle to an asymptotic value. Currents <20 nA mitigated this drift and resulted in much-reduced settling times of a few minutes. The target charging is due to the difference in the current of the incident electrons vs that of the emitted secondaries, which leads to a charge build-up (see the discussion below). This extra charge cannot leave the target in an orderly fashion immediately because the target is an insulator. Most of the nascent ionized electrons do not escape from the bulk and thus do not contribute to the charge imbalance. Over time, steady-state current paths are established in the target that allows the net charge to dissipate into the grounded target frame.

We collected asymmetry datasets (to be described in detail below) in four different configurations by using all combinations of two variables. The first variable was the frequency of the Rb polarizing pump laser; it was either on resonance at a detuning of 1.5 GHz to produce spin-polarized electrons or off-resonance at 12 GHz producing a much more weakly polarized beam. Both of these detunings are relative to the Rb line center of 377.1074 THz. These frequencies resulted in typical electron polarizations of 17(4)% and 3(4)%, respectively. The second variable was the bias voltage applied to the chiral target; it was either -9 V to measure a secondary electron emission signal or $+54$ V to measure the electron beam current incident on the target.

An example of the variation of current measured on the target pins as a function of their bias voltage for a fixed electron flux is shown in Fig. 2. For strongly positive target bias, the electric field surrounding the target attracts any emitted secondary electrons back to the target. The current thus read on the pin corresponds to the incident electron beam current. When the bias is negative, any emitted secondary electrons are repelled from the target so that the measured current corresponds to the summed incident and secondary currents. Because the number of emitted secondary electrons is generally greater than the number of incident electrons,¹⁸ this current is positive. The ratio of emitted secondaries to incident electrons is referred to as the “secondary electron yield,” γ . The current, shown in Fig. 2, for negative bias reaches a maximum between -27 and -36 V and then begins to decline as the bias becomes even more negative, corresponding to a deceleration and deflection of the incident beam away from the target. We measured asymmetries at -9 V in an effort to maximize the sensitivity of the pin current to secondary electron production while minimizing the effects of the negative potential on the incident beam trajectory and energy. We found that $+54$ V was sufficient to capture essentially all the current incident on the pin (as determined by the Faraday cup current) while also suppressing secondary electron emission. By comparing the beam currents measured at -9 and $+54$ V, we could get a rough estimate of the value of the secondary yield using the formula

$$\gamma = \frac{I_{+54} - I_{-9}}{I_{+54}}, \quad (1)$$

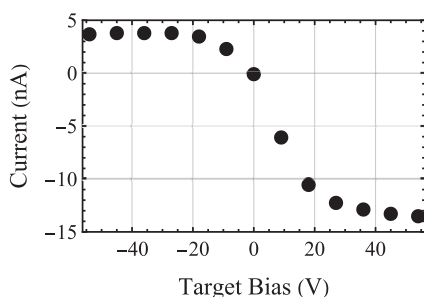


FIG. 2. The current measured on a chiral cysteine target as a function of its bias voltage for an incident electron energy of 150 eV. We can be certain that secondary electrons are being generated because the current is positive when the target has a negative bias. During asymmetry data collection, the target was biased at either -9 or $+54$ V.

where I_{+54} and I_{-9} are the currents measured on the target for biases of $+54$ and -9 V, respectively. The value of γ depends on the primary electron's kinetic energy and its angle of incidence.¹⁸ In this study, the electron beam was fixed at a normal incidence to the surface, and we measured γ as a function of incident electron energy. Typically, γ increases from a value of 0 at ~ 20 eV, the threshold incident electron energy for kinetic emission, to a maximum, generally between 100 and 500 eV. At present, our system is limited to 160 eV; hence, it could not reach the peak of the γ curve.

Figure 3 shows γ at three different incident electron energies with a cysteine target. To our knowledge, the γ values for a solid cysteine surface have not been reported prior to this measurement. These results are not highly accurate, however, because as the incident energy of the electrons is changed, both they and the secondaries they emit will be affected differently by fixed electric fields due to the target bias. Variations in the measured γ may also occur due to the fact that different target holders will exhibit small variations in the biasing fields and that the asymptotic bias voltages needed to ensure that all of the secondaries will be fully rejected or captured will depend on the incident energy as well. This problem is illustrated by the fact that the calculated value of $\gamma = 1.3$ for the data of Fig. 2, which were taken at an incident energy of 150 eV, match poorly with the 160 eV data shown in Fig. 3. We note that the asymmetries we measure and discuss below are asymmetries of the current measured on the target, not γ .

A chiral asymmetry signal associated with the secondary electron emission process is only expected when the pump laser was on resonance (1.5 GHz), and the target was biased at -9 V; the other combinations of measurements determine instrumental asymmetries. These on-resonance and -9 V biased “signal data” were collected twice, once at the beginning of a full dataset and once at the end of the set. The target carriage system was then translated vertically so that the beam was incident on the opposite enantiomer target, and the same data-taking protocol was repeated. This process was repeated for 50 runs of data on seven pairs of chiral targets. We did not measure chiral molecule degradation as a function of exposure but limited the number of measurements on each sample to mitigate the effect this might have had on our results. Having said this, the electron fluence for any given experimental run was $<10^{16} e^-/\text{cm}^2$. When compared with the destruction rates for cysteine measured by Rosenberg *et al.*,¹⁰ we expect that negligible chemical changes will have occurred in the target over the course

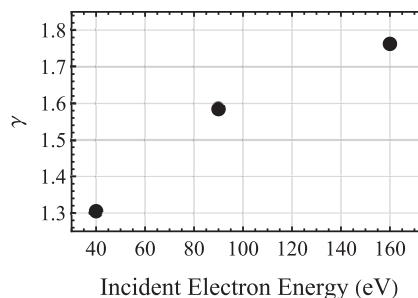


FIG. 3. The secondary electron yield (γ), as a function of the incident electron beam's energy. In its current configuration, the maximum energy of our electron source does not reach the maximum of the secondary yield.

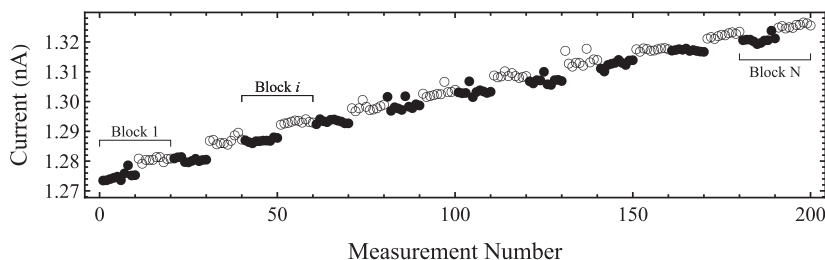


FIG. 4. An example of one asymmetry dataset, collected with -9 V bias, the pump laser on resonance, and the electron beam incident on the *D*-enantiomer of cysteine. It consists of $N = 10$ blocks of $2M = 20$ measurements, where the first ten measurements are collected with one electron polarization, and the second ten are collected with the opposite polarization. The filled circles represent the current collected with spin-forward electrons; the open circles represent the current collected with spin-backward electrons. Specific data blocks discussed in the text are indicated. This dataset gives an overall value of asymmetry $\bar{a} = -1.09(4) \times 10^{-3}$.

of the experiments. This is consistent with the fact that we did not observe any systematic changes in chiral asymmetries over the period that a given target was in use. No visible changes to the target occurred as a result of electron beam exposure.

D. Data analysis

A single asymmetry dataset consisted of $N = 10$ blocks of $2M = 20$ current measurements. In each block, the first ten measurements were collected with one electron polarization and the last ten with the opposite polarization. An example of a raw dataset is shown in Fig. 4. We calculated the asymmetry, b , for each block by taking the average of these M measurements for each polarization, \bar{I} , and using the formula

$$b_i = \frac{\bar{I}_{\uparrow i} - \bar{I}_{\downarrow i}}{\bar{I}_{\uparrow i} + \bar{I}_{\downarrow i}}. \quad (2)$$

Here, the $\uparrow(\downarrow)$ indicates the electron polarization incident on the target, and i indicates the block number out of the total N blocks.

If there is a monotonic drift in the data, this would result in a false asymmetry. The $\sim 5\%$ current drift shown in Fig. 4 is fairly typical for the data we collected. It is not a target charging effect but is rather due to small variations in the primary beam (as determined both by monitoring the filament emission current and that at the Faraday cup). We suspect that the chief culprit here is small movements of the thermionic filament itself, caused by random heating and cooling of the filament at its average temperature. To eliminate this potential error, we calculated a second asymmetry, c , using the same data, but we paired the second part of block i with the first part of block $i + 1$ so that in this second calculation, the opposite polarization is collected first:

$$c_i = \frac{\bar{I}_{\uparrow i+1} - \bar{I}_{\downarrow i}}{\bar{I}_{\uparrow i+1} + \bar{I}_{\downarrow i}}. \quad (3)$$

By pairing the measurements in this way, there is one fewer block of measurements. We then take the average of the first asymmetry and second asymmetry values, dropping the first block from the first set of asymmetries so that there are an equal number of calculations with each pump light helicity collected first. The average of these

nine measurements, \bar{a} , is the overall asymmetry that we report for a single dataset:

$$\bar{a} = \sum_{i=1}^{N-1} \frac{b_{i+1} + c_i}{2}. \quad (4)$$

An example of this analysis is shown in Fig. 5.

In rare cases, the electron beam current fluctuated strongly during the course of a measurement. This resulted in false asymmetries that were clearly caused by these transient effects. To systematically eliminate these fluctuations, the analysis code calculated the difference between each successive current measurement. It then automatically removed from the above sum any of the i blocks that contained an instance of the current measurement varying by more than five standard deviations from the average difference between measurements.

There are significant instrumental asymmetries as can be seen in Fig. 6. We combined the asymmetries measured with both enantiomers into a value A that we call “the chiral sample asymmetry” to reduce these effects. The difference of the \bar{a} values measured for each enantiomer is

$$A = \bar{a}_D - \bar{a}_L, \quad (5)$$

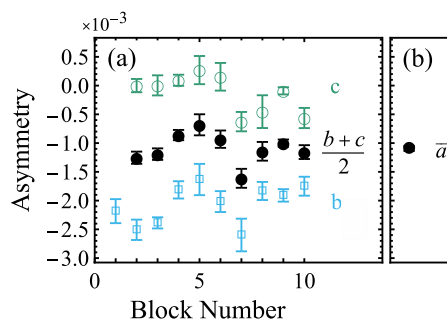


FIG. 5. An example application of the drift correction process applied to the data of Fig. 4. In (a), the open squares are the b value obtained from Eq. (2), the open circles are the c values obtained from Eq. (3), and the filled circles are the average of these two methods. In (b), the value of \bar{a} is indicated, the result of Eq. (4), representing the overall asymmetry of the dataset.

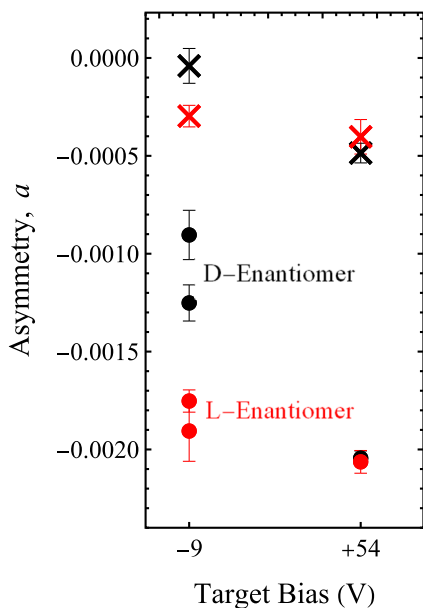


FIG. 6. The measured asymmetry values, a , were influenced by the experimental parameters of the system. The cross marks show the asymmetry measured when the pump laser was off-resonance, which was significantly different than the value with the laser on resonance, shown by the filled circles. The -9 or $+54$ V bias of the targets can also be seen to affect the asymmetry that was measured. The different colored markers represent measurements collected on the D - and L -targets as labeled in the figure. These data represent the values obtained from one run of data.

where D (L) refers to the dextrorotary (levorotary) enantiomer. We calculated an A value for each of the four configurations discussed earlier, that is $A_{\text{on},-9}$, $A_{\text{off},-9}$, $A_{\text{on},+54}$, and $A_{\text{off},+54}$, where the subscript labels the “on” or “off” resonance condition for the Rb pump light frequency, and -9 or $+54$ refer to the target bias voltage. The chiral signal when the beam is off-resonance should be negligible, since

electron polarization is more than five times smaller. We thus subtract the off-resonance value from the on-resonance value and divide by P_e , the average electron polarization measured for the runs on that day, since we expect the measured asymmetry to scale with the electron polarization. This gives our final values of the asymmetry:

$$A_{-9} = \frac{A_{\text{on},-9} - A_{\text{off},-9}}{P_e}, \quad (6)$$

and

$$A_{+54} = \frac{A_{\text{on},+54} - A_{\text{off},+54}}{P_e}. \quad (7)$$

If a chiral asymmetry exists, we expect it to be present in the -9 V data and absent in the $+54$ V data. The two pin bias voltages result in different collision energies (132 vs 195 eV) that could, in principle, affect the result of our asymmetry measurements. We expect this effect to be small, given that it corresponds to only a $\sim 6\%$ change in γ , and A_{+54} is expected to be small in any case. As an additional control, we collected datasets where both targets were the same enantiomer. In these measurements, the value of A in Eq. (5) should always be zero. Any deviation from zero would be caused by instrumental asymmetries.

Our value for the asymmetry in the collision process is the average of 49 datasets. One run was excluded from the results after applying Chauvenet’s criterion.³⁰ The error in the measurement is the standard deviation of the mean of the values. The full collection of measured asymmetries is shown in Fig. 7.

III. RESULTS AND DISCUSSION

Our final results are shown in Fig. 8. The composite value for A_{-9} is consistent with zero, indicating that we observe no electron spin-dependent effect in secondary electron emission from isotropic cysteine thick films at a level of 10^{-3} . We considered doing a series of experiments with racemic mixtures of L - and D -cysteine to confirm this null result, but the “same enantiomer control” result, also shown in Fig. 8, seemed to obviate the need for this measurement.

What limits our experiment to an overall precision of $\sim 10^{-3}$? Drifting of the type shown in Fig. 4 does not contribute significantly

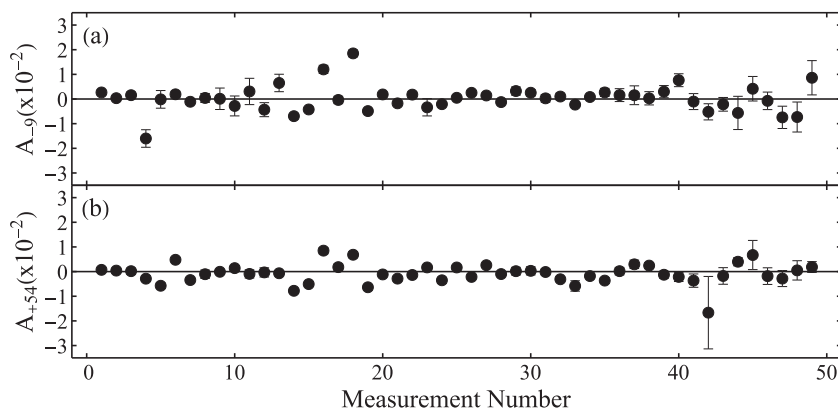


FIG. 7. Summary of the measured asymmetries [Eq. (6) for (a); Eq. (7) for (b)] that were combined to yield the final results shown in Fig. 8. This displays the instrumental fluctuations characteristic of our apparatus that determine the final uncertainties we report.

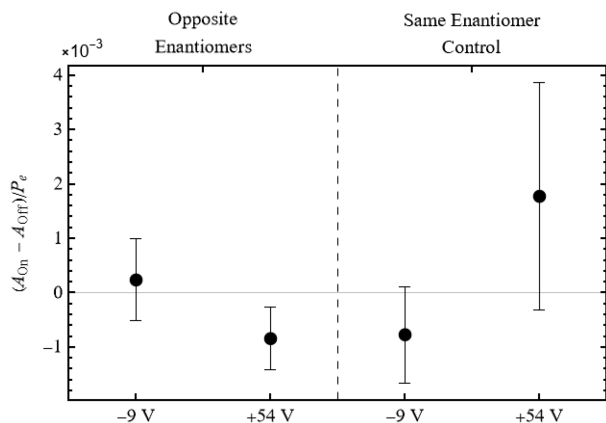


FIG. 8. Asymmetry values associated with secondary electron production in spin-polarized electron collisions with the amino acid cysteine reflect the full set of data collected in this experiment. The data points represent the background-subtracted chiral asymmetry defined by Eqs. (6) and (7) (see text). The labels on the abscissa indicate the bias applied to the chiral target. “Same Enantiomer Control” refers to experiments in which both targets had the same handedness (see text).

to this value. This is evident from the final asymmetry \bar{a} [Fig. 5(b)], which has an uncertainty of $\sim 10^{-4}$. (See also Fig. 7 in this regard, where most of the individual run asymmetries have a precision better than the size of the data points.) There are, however, two issues with the data, neither of which we completely understand at this point. These are illustrated in Fig. 6. Any asymmetries measured at +54 V should be zero, since we are sensitive only to total beam current at that voltage. The asymmetries measured with a detuned laser should also be zero, since incident electron polarization is very low in this case. (We note that for either bias voltage, the measured target current does not change when we detune the pump laser.) However, we find that both of these instrumental asymmetries are statistically different from zero. Moreover, they vary from run to run and from target to target. Not having a clear understanding of why this happens, we are forced to adopt the procedure discussed in Sec. II D. Thus, our final error bars are not statistical in nature but result from the standard error of the run data shown in Fig. 7, which is essentially a heuristic uncertainty due to the run-to-run variability of the instrumental asymmetries. It is this variability that limits our ultimate experimental precision.

The uncertainty of this measurement is relatively large compared with the expected size of the effect in gaseous targets (10^{-4} – 10^{-3}). Cysteine contains a sulfur atom with a relatively high Z value (16), but it is smaller than that of the molecules we investigated in earlier experiments⁸ in which a spin-dependent collision asymmetry was observed. The scaling of the asymmetry measurement with Z^2 in Fig. 5 of Ref. 8 implies that our cysteine experiment should have an asymmetry of $\sim 6 \times 10^{-5}$ for single collision conditions; the earlier experiments used gaseous targets. It is reasonable to expect that the condensed nature of the solid cysteine might make up for the effect of having lower Z , but this was not the case. Selenocysteine is a candidate for a molecule that would increase the value of Z (34) for a future search, possibly giving a Z -scaled value of 2×10^{-4} . Observation of this asymmetry would require

experimental measurements with a precision of at least five times better than those reported here.

Another target to try might be iodocamphor. In our previous gas-phase measurements, the dissociative electron attachment (DEA) channel exhibited a chiral asymmetry of $\sim 2 \times 10^{-3}$ with this molecule. If this were to carry over to the secondary-electron emission channel, it would be marginally detectable with the apparatus sensitivity demonstrated by the measurements discussed here. We avoided this target in the first round of experiments because of the time and expense involved in its fabrication, and our desire to investigate a more biologically relevant target.

Experiments conducted with gas-phase targets or the randomly oriented molecular solids of the type considered here have the advantage that any asymmetry observed is a clean signature of electron-molecular chiral interactions, devoid of any underlying geometric chirality associated with the experimental geometry. The disadvantage of such measurements is that the asymmetries that are measurable tend to be small. We initially hoped that (unlike gas-phase experiments) the large number of interactions that occur in a solid and that result in secondary electron emission might have had an additive effect resulting in a measurable asymmetry, in the same way, that rather large asymmetries have been observed in solid (albeit more ordered) films of DNA and butanol.^{11,17} Ultimately, our null result is probably due to a combination of the target’s random molecular orientation, its relatively low Z , and, possibly most importantly, the high incident electron energy needed to initiate kinetic secondary electron emission. To be sure, the primary electron ultimately slows down to the extent that chiral effects could become important in the production of ionized electrons, but this occurs at the end of its track, where the emission probability of an ionized electron is minimized.

IV. CONCLUSION

We have attempted to measure a chirality-dependent asymmetry in the kinetic secondary electron emission resulting from longitudinally spin-polarized electrons incident on solid cysteine. More broadly, the role of chiral interactions in electron–molecule collisions is not well understood, and additional data are needed to further understand these processes. These results expand the database for electron-chiral interactions by including the channel of secondary electron emission but show no effect at the level of 10^{-3} . Nonetheless, this null result provides a useful upper limit for chiral effects in a collision channel not previously studied. This is also the first measurement reported where a Rb spin-exchange source was used as a source of spin-polarized electrons.

The increased cross-section involved with a solid target and the lack of existing measurements on this particular interaction channel encourage us to perform further measurements with higher Z targets and improved methods to increase the accuracy and precision with which we can characterize the importance of chiral interactions in kinetic secondary electron emission.

ACKNOWLEDGMENTS

This work was supported by the U.S. NSF with Award No. PHY-2110358. The research was performed in part in the Nebraska

Nanoscale Facility: National Nanotechnology Coordinated Infrastructure and the Nebraska Center for Materials and Nanoscience, which are supported by the National Science Foundation under Award No. ECCS: 2025298, and the Nebraska Research Initiative.

AUTHOR DECLARATIONS

Conflict of Interest

The authors have no conflicts to disclose.

Author Contributions

K. J. Ahrendsen: Formal analysis (equal); Writing – original draft (equal); Writing – review & editing (equal). **K. W. Trantham:** Investigation (equal); Methodology (equal); Software (equal); Supervision (equal); Writing – review & editing (equal). **D. Tupa:** Formal analysis (equal); Writing – review & editing (equal). **T. J. Gay:** Conceptualization (equal); Formal analysis (equal); Project administration (equal); Writing – review & editing (equal).

DATA AVAILABILITY

The data that support the findings of this study are available from the corresponding author upon reasonable request.

REFERENCES

- ¹S. F. Mason, “Molecular handedness and the origins of chiral discrimination,” *Int. Rev. Phys. Chem.* **3**, 217–241 (1983).
- ²T. L. V. Ulbricht, “Asymmetry: The non-conservation of parity and optical activity,” *Q. Rev., Chem. Soc.* **13**, 48–60 (1959).
- ³C. S. Wu, E. Ambler, R. W. Hayward, D. D. Hoppes, and R. P. Hudson, “Experimental test of parity conservation in beta decay,” *Phys. Rev.* **105**, 1413–1415 (1957).
- ⁴W. A. Bonner, M. A. Van Dort, and M. R. Yearian, “Asymmetric degradation of DL-leucine with longitudinally polarised electrons,” *Nature* **258**, 419–421 (1975).
- ⁵B. Boudaïffa, P. Cloutier, D. Hunting, M. A. Huels, and L. Sanche, “Resonant formation of DNA strand breaks by low-energy (3 to 20 eV) electrons,” *Science* **287**, 1658–1660 (2000).
- ⁶J. M. Dreiling and T. J. Gay, “Chirally sensitive electron-induced molecular breakup and the Vester-Ulbricht hypothesis,” *Phys. Rev. Lett.* **113**, 118103 (2014).
- ⁷C. Nolting, S. Mayer, and J. Kessler, “Electron dichroism—new data and an experimental cross-check,” *J. Phys. B: At., Mol. Opt. Phys.* **30**, 5491–5499 (1997).
- ⁸J. M. Dreiling, F. W. Lewis, and T. J. Gay, “Spin-polarized electron transmission through chiral halocamphor molecules,” *J. Phys. B: At., Mol. Opt. Phys.* **51**, 21LT01 (2018).
- ⁹K. W. Trantham, M. E. Johnston, and T. J. Gay, “Failure to observe electron circular dichroism in camphor,” *J. Phys. B: At., Mol. Opt. Phys.* **28**, L543 (1995).
- ¹⁰R. A. Rosenberg, E. A. Rozhkova, and V. Novosad, “Investigations into spin- and unpolarized secondary electron-induced reactions in self-assembled monolayers of cysteine,” *Langmuir* **37**, 2985–2992 (2021).
- ¹¹B. Göhler, V. Hamelbeck, T. Z. Markus, M. Kettner, G. F. Hanne, Z. Vager, R. Naaman, and H. Zacharias, “Spin selectivity in electron transmission through self-assembled monolayers of double-stranded DNA,” *Science* **331**, 894–897 (2011).
- ¹²M. J. Schaible, R. A. Rosenberg, S. Kundu, and T. M. Orlando, “Electron spin-polarization dependent damage to chiral amino acid L-histidine,” *J. Phys. Chem. Lett.* **11**, 10182–10187 (2020).
- ¹³P. C. Mondal, C. Fontanesi, D. H. Waldeck, and R. Naaman, “Spin-dependent transport through chiral molecules studied by spin-dependent electrochemistry,” *Acc. Chem. Res.* **49**, 2560–2568 (2016).
- ¹⁴D. T. Pierce, R. J. Celotta, G.-C. Wang, W. N. Unertl, A. Galejs, C. E. Kuyatt, and S. R. Mielczarek, “The GaAs spin polarized electron source,” *Rev. Sci. Instrum.* **51**, 478–499 (1980).
- ¹⁵H. Batelaan, A. S. Green, B. A. Hitt, and T. J. Gay, “Optically pumped electron spin filter,” *Phys. Rev. Lett.* **82**, 4216–4219 (1999).
- ¹⁶M. Pirbhaj, J. Knepper, E. T. Litaker, D. Tupa, and T. J. Gay, “Optically pumped spin-exchange polarized-electron source,” *Phys. Rev. A* **88**, 060701 (2013).
- ¹⁷R. A. Rosenberg, M. Abu Haija, and P. J. Ryan, “Chiral-selective chemistry induced by spin-polarized secondary electrons from a magnetic substrate,” *Phys. Rev. Lett.* **101**, 178301 (2008).
- ¹⁸A. J. Dekker, *Solid State Physics* (Macmillan International Higher Education, 1969).
- ¹⁹K. J. Ahrendsen, K. W. Trantham, D. Tupa, and T. J. Gay, “An improved source of spin-polarized electrons based on spin-exchange in an optically-pumped rubidium vapor” (unpublished) (2022).
- ²⁰M. Pirbhaj, D. M. Ryan, G. Richards, and T. J. Gay, “Compact inline optical electron polarimeter,” *Rev. Sci. Instrum.* **84**, 053113 (2013).
- ²¹R. G. Nuzzo and D. L. Allara, “Adsorption of bifunctional organic disulfides on gold surfaces,” *J. Am. Chem. Soc.* **105**, 4481–4483 (1983).
- ²²K. Uvdal, P. Bodö, and B. Liedberg, “L-cysteine adsorbed on gold and copper: An X-ray photoelectron spectroscopy study,” *J. Colloid Interface Sci.* **149**, 162–173 (1992).
- ²³M. P. Seah and W. A. Dench, “Quantitative electron spectroscopy of surfaces: A standard data base for electron inelastic mean free paths in solids,” *Surf. Interface Anal.* **1**, 2–11 (1979).
- ²⁴I. M. Weiss, C. Muth, R. Drumm, and H. O. K. Kirchner, “Thermal decomposition of the amino acids glycine, cysteine, aspartic acid, asparagine, glutamic acid, glutamine, arginine and histidine,” *BMC Biophys.* **11**, 2 (2018).
- ²⁵A. Stamatovic and G. J. Schulz, “Trochoidal electron monochromator,” *Rev. Sci. Instrum.* **39**, 1752–1753 (1968).
- ²⁶T. J. Gay, “A simple optical electron polarimeter,” *J. Phys. B: At. Mol. Phys.* **16**, L553–L556 (1983).
- ²⁷H. G. Berry, G. Gabrielse, and A. E. Livingston, “Measurement of the Stokes parameters of light,” *Appl. Opt.* **16**, 3200 (1977).
- ²⁸Z. Wu, M. Kitano, W. Happer, M. Hou, and J. Daniels, “Optical determination of alkali metal vapor number density using Faraday rotation,” *Appl. Opt.* **25**, 4483 (1986).
- ²⁹A. Ueno, K. Takasaki, K. Ogura, Y. Wakuta, I. Kumabe, K. O-Ohata, Y. Mori, and S. Fukumoto, “Faraday rotation of optically pumped sodium vapour in a weak magnetic field,” *Nucl. Instrum. Methods Phys. Res., Sect. A* **262**, 170–178 (1987).
- ³⁰P. Bevington and D. Robinson, *Data Reduction and Error Analysis for the Physical Sciences* (McGraw-Hill Education, 2003).